EXPERIMENTAL CELL RESEARCH 317 (2011) 2823–2834

Available online at www.sciencedirect.com

SciVerse ScienceDirect

www.elsevier.com/locate/yexcr

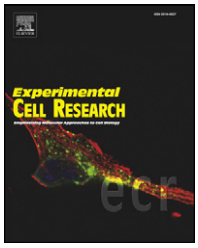

Research Article

RhoA–ROCK–Myosin pathway regulates morphological plasticity of cultured olfactory ensheathing cells

Zhi-hui Huang[a,b,1], *Ying Wang*[a,b,1], *Xiao-bing Yuan*[c,*], *Cheng He*[a,b,**]

[a] *Institute of Hypoxia Medicine, Wenzhou Medical College, Wenzhou, Zhejiang 325035, China*
[b] *Institute of Neuroscience and Key Laboratory of Molecular Neurobiology of Ministry of Education, Neuroscience Research Center of Changzheng Hospital, Second Military Medical University, Shanghai 200433, China*
[c] *Institute of Neuroscience and State Key Laboratory of Neuroscience, Chinese Academy of Sciences, Shanghai 200031, China*

ARTICLE INFORMATION

Article Chronology:
Received 2 April 2011
Revised version received 9 August 2011
Accepted 9 September 2011
Available online 17 September 2011

Keywords:
Olfactory ensheathing cells
RhoA
Morphological plasticity
Regeneration
Myosin

ABSTRACT

Olfactory ensheathing cells (OECs) are glial cells in the olfactory system with morphological and functional plasticity. Cultured OECs have the flattened and process-bearing shape. Reversible changes have been found between these two morphological phenotypes. However, the molecular mechanism underlying the regulation of their morphological plasticity remains elusive. Using RhoA FRET biosensor, we found that the active RhoA signal mainly distributed in the lamellipodia and/or filopodia of OECs. Local disruption of these active RhoA distributions led to the morphological change from the flattened into process-bearing shape and promoted process outgrowth. Furthermore, RhoA pathway inhibitors, Toxin-B, C3, Y-27632 or over-expression of DN-RhoA blocked serum-induced morphological change of OECs from the process-bearing into flattened shape, whereas the activation of RhoA pathway by lysophosphatidic acid (LPA) promoted the morphological change from the process-bearing into flattened shape. Finally, ROCK–Myosin–F-actin as a downstream of RhoA pathway was involved in morphological plasticity of OECs. Taken together, these results suggest that RhoA–ROCK–Myosin pathway mediates the morphological plasticity of cultured OECs in response to extracellular cues.

© 2011 Elsevier Inc. All rights reserved.

Introduction

Olfactory ensheathing cells (OECs) are a type of glial cells in the olfactory system with axonal growth-promoting properties. They have been discovered to promote the growth of olfactory sensory axons and the regeneration of injured axons after being transplanted into nerve injury sites [1,2]. Current studies have shown that OECs have enormous potential for therapeutic use in treatment of axonal injuries and demyelinating diseases [3–7].

Initially, cultured OECs are described as antigenically and morphologically heterogeneous and comprised of both astrocyte-like cells and Schwann cell-like cells [4,8–11]. However, recent studies have shown that cultured OECs are a single cell type with morphological plasticity [12–15]. Cultured OECs have flattened shape with a flat sheet-like

* *Corresponding author.*
** *Correspondence to:* C. He, Institute of Neuroscience and Key Laboratory of Molecular Neurobiology of Ministry of Education, Neuroscience Research Center of Changzheng Hospital, Second Military Medical University, Shanghai 200433, China. Fax: +86 21 65492132.
E-mail addresses: yuanxb@ion.ac.cn (X. Yuan), chenghe@smmu.edu.cn (C. He).

Abbreviations: OECs, Olfactory ensheathing cells; FBS, fetal bovine serum; PLL, poly-L-lysine; LPA, lysophosphatidic acid; FRET, fluorescence resonance energy transfer; ROCK, Rho associated kinase; MLC, myosin light chain.

[1] These authors contributed equally to this work.

0014-4827/$ – see front matter © 2011 Elsevier Inc. All rights reserved.
doi:10.1016/j.yexcr.2011.09.004

morphology and process-bearing shape with a long fusiform bipolar or multi-polar morphology. The morphology of OECs is affected by some extracellular factors such as cultured media [10,14,16–18], endothelin-1 [14] and extracellular matrix [19,20], and intracellular factors such as cAMP [12,14,16,18]. Interestingly, several studies have shown that reversible changes have been found between these two shapes by using time-lapse imaging or addition of cAMP or endothelin-1 [12,14,15]. However, the molecular mechanism underlying the regulation of these reversible changes is still unknown.

The Rho subfamily of small GTPases (including RhoA, Rac1 and Cdc42) are the central players in cell morphology and motility in many cell types through regulating the assembly of actin cytoskeleton, adhesion formation and membrane protrusion. RhoA signals in the formation and maturation of focal adhesion complex associated with actin stress fiber bundles, whereas Rac1 and Cdc42 stimulate the formation of cell protrusions in association with filopodia and lamellipodia [21,22]. RhoA signaling pathways have been reported in mediating the guidance of OEC migration [23–25]. However, whether RhoA pathway regulates the morphological plasticity of cultured OECs remains unclear. In the present study, we demonstrate the role of RhoA signaling pathway in the morphological plasticity of OECs.

Materials and methods

Primary culture of olfactory ensheathing cells

Primary culture of OECs were prepared from olfactory bulb of adult male Sprague–Dawley rats and purified by differential cell adhesiveness as described previously [12,26–29]. Briefly, the meninges were carefully removed from the olfactory bulb under the dissecting microscope and the olfactory nerve layer was peeled away from the glomerular and deeper layers of the olfactory bulb, then dissociated with 0.125% trypsin (Sigma, St Louis, MO) and incubated at 37 °C for 15 min. Trypsinization was stopped by DMEM/F12 (1:1, vol/vol, Gibco, Grand Island, NY) containing 10% heat-inactivated fetal bovine serum (FBS, Hyclone, Logan, UT). The tissue was centrifuged for 10 min at 500 *g*, and the pellet was triturated using a flame-polished Pasteur pipette and plated on uncoated 25 cm^2 culture flask (Corning, LY) two times, each for 36 h at 37 °C in 5% CO_2. The non-adhesive cell suspension was collected and then seeded onto 12-well plates (Corning) pre-coated with poly-L-lysine (PLL, 0.1 mg/ml, Sigma), and incubated with DMEM/F-12 containing 10% FBS, 2 μM forskolin (Sigma) and 10 ng/ml bFGF-2 (Sigma) as mitogen. The media were changed every 3 days. For experiments, the purified OEC cells were replanted onto square coverslips (8 mm) coated with laminin (10 μg/ml) at a density of 2×10^5 cells. OECs were identified by double immunostaining for p-75 and GFAP, or p-75 and S-100, or S-100 and GFAP (Fig. S1). The overall purity of OECs was around 95%. We adopted the previous criteria and method to define and count morphological phenotypes of OECs [12,14]. Process-bearing shape of OECs had very little cytoplasm and two or more fine processes that were longer than the width of the cell body, and flattened shape of OECs had a large area of cytoplasm surrounding the nucleus and either fewer than two processes or processes that were shorter than the width of the cell body. According to these criterions, we counted the total number of each morphological phenotype under bright filed microscopy, and counted the number of positive cells expressed OECs markers at same field under fluorescence microscopy. The purity of each morphological phenotype of OECs was analyzed by determining the percentage of cells expressing OEC marker (p-75, S-100, GFAP) in total counted cells. Quantitative data were from three different cell cultures. Cells were counted in at least 20 randomly selected fields from one coverslip and 100 cells for each shape per coverslip ($n=4$) were counted.

FRET-based imaging of active RhoA with three-channel microscopy

The fluorescence resonance energy transfer (FRET) probe pRaichu-RhoA (YFP–RBD–RhoA–CFP) for monitoring the subcellular RhoA activity was kindly provided by Dr. M. Matsuda (Osaka University) [30]. Cells transfected with the FRET probe were imaged on a Nikon Ti microscope with a 40 oil lens (N.A. 1.30) using the Perfect Focus System and were illuminated by a polychrome IV monochromator (TILL Photonics). Filter sets for FRET imaging are CFP (excitation 436 nm, emission, 480/40 HQ, DM 455), FRET (excitation 436 nm, emission, 535/30 HQ, DM 515) and YFP (excitation 510 nm, emission, 535/30 HQ, DM 515). Images of the three channels were recorded simultaneously by using the Cascade 512B CCD (Roper Scientific). Background images were subtracted from the raw images before carrying out FRET calculation. Corrected FRET ($FRET^C$) was calculated on a pixel-by-pixel basis for the image using the following equation: $FRET^C = FRET\text{-}a\times YFP\text{-}b\times CFP$, where FRET, CFP and YFP corresponded to background-subtracted images, acquired through the FRET, CFP and YFP channels, respectively. "a" and "b" were the fraction of bleed-through of YFP and CFP fluorescence through the FRET channel, respectively, and the two values were determined by using cells transfected with YFP or CFP alone. We used the following equation: $E = FRET^C/(CFP + FRET^C)\times 100\%$ to quantify the FRET signal by using MetaFluo and Image J software (PixFRET Plug-in) [31–33].

Immunocytochemistry and cytoskeleton staining

Briefly, OECs were fixed with fresh 4% paraformaldehyde in 0.1 M PBS (pH 7.4) for 20 min. After washed by PBS, cells were permeabilized with 0.2% Triton X-100 in 0.1 M PBS for 5 min, followed by incubation in blocking buffer (5% normal goat serum and 0.2% Triton X-100 in 0.1 M PBS, pH 7.4) for 1 h, and incubated overnight at 4 °C with polyclonal antibodies against p-75 (1:500, Promega, Madison, WI), or GFAP (1:500, Sigma) and with a monoclonal anti-p-MLC antibody (1:200, Cell Signaling Technology) or anti-S-100 antibody (1:500, Sigma) or anti-p-75 antibody (1:200, Chemicon), diluted in the blocking buffer. Cells were washed three times with PBS and incubated for 1 h at room temperature with an appropriate fluorescence-conjugated secondary antibody (1:1000, Molecular probe, Eugene, OR), and then visualized by confocal fluorescence microscopy (FV1, 000, Olympus). No positive signal was observed in control incubations with no primary antibody. For visualization of F-actin, cells were incubated with rhodamine-conjugated phalloidin (1:60, Molecular probe) at room temperature for 1 h.

Plasmids and cell transfection

EGFP-tagged WT-RhoA and DN-RhoA were used previously [34]. For cultured OEC transfection, we used rat Astrocyte Nucleofector Kit (Amaxa) according to the manufacturer's instructions. Briefly,

dissociated cells were re-suspended in transfection medium, mixed with plasmid (3 μg), and electroporated using the fixed program (T-20). Cells were then quickly re-suspended and planted. The media were changed 4 h after transfection, and cells were used for experiments 24 h after transfection.

Drugs

Drugs were purchased from companies as follows: bacterial endotoxin C3 exoenzyme (C3) (Cytoskeleton, USA), Toxin-B, Y-27632 and Blebbistatin (Calbiochem, La Jolla, CA). OECs were re-plated onto square coverslips coated with laminin (10 μg/ml) for 24 h under serum condition without bFGF and forskolin, and then OECs were treated with Toxin-B for overnight, or C3 for at least 6 h, or Y-27632 or Blebbistatin for at least 2 h under different concentrations.

Micropipette assays based on time-lapse imaging

The gradients of factors were produced as described previously [12,34]. Briefly, the purified OEC cells were replanted onto the square coverslips (8 mm) coated with laminin (10 μg/ml) at a low density of 1000 cells per coverslip. Twenty-four hours after planting, coverslip was put into a chamber containing 1 ml serum-free Leibovitz's L-15 medium (L15, Gibco). The chamber was then covered with a thin layer of methyl-siloxane fluid to prevent water evaporation. The experiments were carried out at heated stage (37 °C) of a phase contrast microscope (CK40, Olympus optical, Tokyo, Japan). Cells with a typical morphology of OECs and without attaching with any other cells were selected. The micropipette was controlled by the 3D micromanipulator. A micropipette with a tip opening of about 1 μm was placed at 15 μm perpendicular and about 100 μm away from the center of the cell body under test. A standard pressure pulse of 3 psi (1 psi = 6.89 kPa) in amplitude and 20 ms in duration, was generated by a pulse generator and applied to the pipette at a frequency of 2 Hz. Images of OECs were recorded, in a time-lapse mode (one picture/5 min interval, total time 60 min), with a CCD camera (JVC TK-1381; Victor Company, Yokohama, Japan) attached to the microscope and stored in a computer. The braches and the total length of leading and trailing processes in OECs were calculated by using Scion image software (Frederick, MD).

Pull-down assay of active RhoA

For analyzing RhoA activity in cell lysates, an activated RhoA pull-down kit was used with following protocols provided by the manufactory (Cytoskeleton, USA). Briefly, cultured OECs were starved for overnight, then stimulated by 10% serum or 10 μM LPA before lysed in 250 μl of the supplied lysis buffer containing protease inhibitor cocktail. About 20 μl of each lysate was used for protein quantification and western blotting analysis of total RhoA. For the rest of lysates, a volume of equal protein amounts from each sample were incubated with Rhotekin-RBD affinity beads for 1 h at 4 °C, followed by two washes in the wash buffer. Bound proteins were collected and examined by 12% SDS-PAGE for western blotting analysis.

Statistical analysis

All data presented represent results from at least three independent experiments. Statistical analysis was performed using Student's *t*-test or ANOVA with pair-wise comparisons. Statistical significance was defined as $P<0.05$.

Results

The distribution of active RhoA in cultured OECs

Consistent with previous studies [12,14,26–29], primary cultured OECs displayed mainly two kinds of morphology, flattened and process-bearing shape. We adopted the previous criteria and method to define and count the morphological phenotypes of OECs [12,14]. Cultured OECs were identified by double immunostaining for p-75 and GFAP, or p-75 and S-100, or S-100 and GFAP, cell markers of OECs. Most of process-bearing and flattened OECs were immunopositive for p-75 and GFAP, or p-75 and S-100, or S-100 and GFAP (Supplementary data, Fig. S1). The overall purity of OECs was around 95%.

To explore the potential effects of RhoA on OEC morphology, we first examined the distribution of active RhoA in OECs. Cultured OECs were transfected with a fluorescence resonance energy transfer (FRET)-based biosensor pRichu-RhoA [30], which was constructed by linking CFP-conjugated RhoA and YFP-conjugated RhoA-binding domain (RBD) of Rhotekin, a configuration sensitive to the activation of RhoA by guanine nucleotide exchange factor. As shown in Fig. 1A, the FRET signal for the active RhoA displayed a polarized distribution in a process-bearing OEC, with the leading and trailing process exhibiting higher activity than the soma. The average FRET efficiency showed no significant difference between the leading and trailing process (Fig. 1C). In a flattened OEC, the active RhoA signal displayed a diffused distribution (Fig. 1B), in the whole lamellipodia and/or filopodia. These results suggest that active RhoA mainly distributes in the lamellipodia and/or filopodia of OECs, but not in the soma. This notion was further supported by the photometric analysis of the active RhoA in OECs based on time-lapse imaging. In the migrating process-bearing OEC, the activity of RhoA was increased in membrane protrusion, and maintained this polarized distribution (Fig. 1D). In the flattened OEC underwent migration, the active RhoA still displayed the diffused distribution (Fig. 1E). The distribution of active RhoA in lamellipodia and/or filopodia may be critical to maintain the morphological phenotypes of OECs.

Inhibition of RhoA pathway by a Y-27632 gradient promotes more and longer processes in OECs

To examine the effects of RhoA on OEC morphology, we observed the morphological change of a single OEC, whose RhoA signaling pathway was locally inhibited by a gradient of Y-27632, a specific Rho associated kinase (ROCK) inhibitor, based on micropipette assays. One typical OEC with two processes, the leading process and trailing process, was selected for the assay. When a gradient of Y-27632 was applied in front of this cell, the leading process gradually grew into three thinner and longer branches, and the trailing process also became thinner and longer (Fig. 2B), compared with during control period. In contrast, the morphology of process-bearing OECs did not change under PBS gradient (Fig. 2A). Statistical analysis showed that the number of branches and total length of processes (including the leading and trailing)

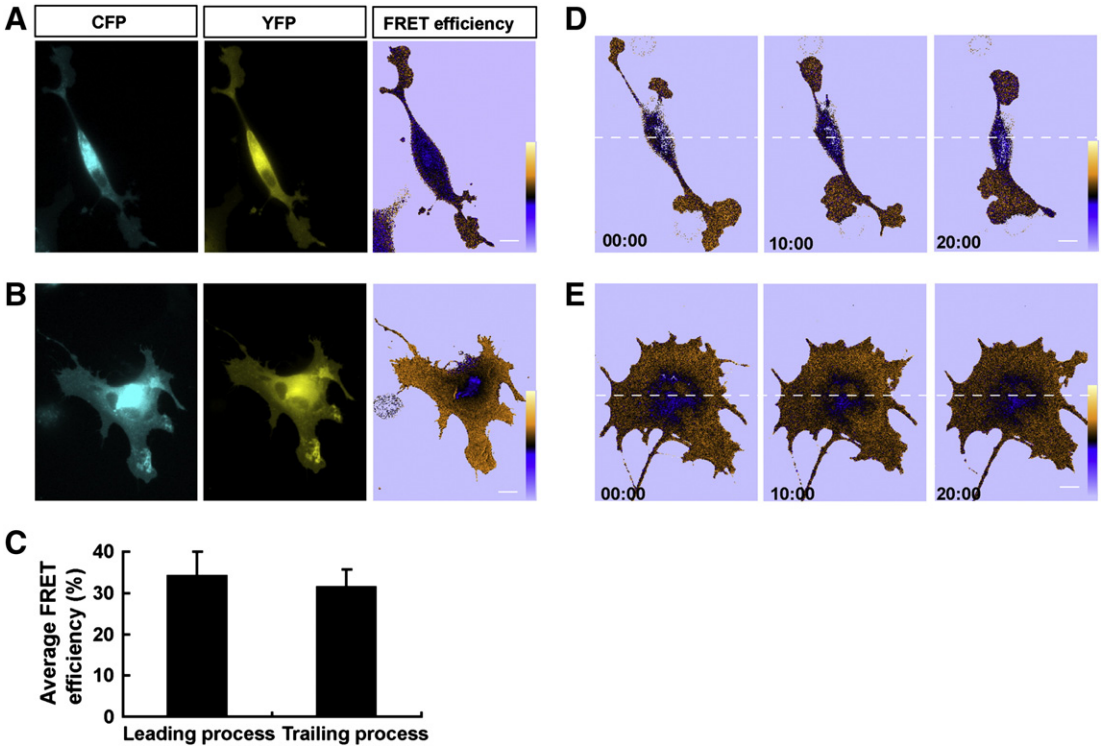

Fig. 1 – The distribution of active RhoA in OECs. (A–B) Representative FRET images with three-channel microscopy show the distribution of active RhoA in cultured OECs with process-bearing shape (A) and flattened shape (B). (C) Statistical analysis of the average FRET efficiency in leading and trailing process of OECs (n = 11). (D–E) Images show dynamic FRET signal (in pseudocolors) in the migrating OECs with process-bearing shape (D) and flattened shape (E). Scale bars, 20 μm. Time, minutes.

were increased significantly under Y-27632 gradient, compared with control (Figs. 2C–D). These results suggest that the inhibition of RhoA pathway could promote more and longer processes in OECs.

Inhibition of RhoA pathway by a Y-27632 gradient induces the morphological change from the flattened into process-bearing shape

We next examined the morphological change in flattened OECs under the inhibition of RhoA pathways. One typical OEC with flattened shape was selected and its morphology did not change during control time. After the application of a gradient of Y-27632 by the micropipette, the large lamellipodia gradually became longer and thinner processes and finally transformed into a typical processing-bearing OEC (Fig. 3B). In contrast, the morphology of OECs did not change upon the application of a PBS gradient (Fig. 3A). We found that 19/20 of OECs with flattened shape transformed into process-bearing shape under Y-27632 gradient, while only 3/24 of OECs with flattened shape could spontaneously transform into process-bearing morphology under the PBS gradient (Fig. 3C). The number of process also increased significantly under Y-27632, compared to PBS (Fig. 3D). These results strongly suggest that inhibition of RhoA pathway is sufficient to induce the morphological change of OECs from the flattened into process-bearing shape.

Over-expression of WT-RhoA or DN-RhoA induces the morphological change of OECs

Further experiments were carried out in OECs transfected with constructs expressing fusion proteins EGFP-wide-type-RhoA (EGFP-WT-RhoA) and EGFP-dominant-negative RhoA (EGFP-DN-RhoA). When cultured OECs were transfected with control construct EGFP, 39.4 ± 6.5% of OECs were flattened morphology, and 60.6 ± 6.5% of OECs were multi-polar, process-bearing morphology (Figs. 4A, D). However, when OECs were transfected with EGFP-WT-RhoA, the percentage of the flattened was significantly increased, 89.3 ± 6.1% of these cells adopted the flattened morphology (Figs. 4B, D). In contrast, after over-expression of EGFP-DN-RhoA, the percentage of the process-bearing was significantly increased, 84.4 ± 16.6% of OECs exhibited multi-polar, process-bearing morphology (Figs. 4C–D). These results suggest that RhoA is critical for the morphology of OECs.

RhoA pathway is required for serum-induced morphological change of OECs

Previous studies have shown that OECs have multipolar, process-bearing morphology in the absence of serum and large, flattened morphology in the presence of serum [10,14,17]. We next examined whether RhoA is required for serum-induced morphological change of OECs. Consistent with these previous studies, OECs

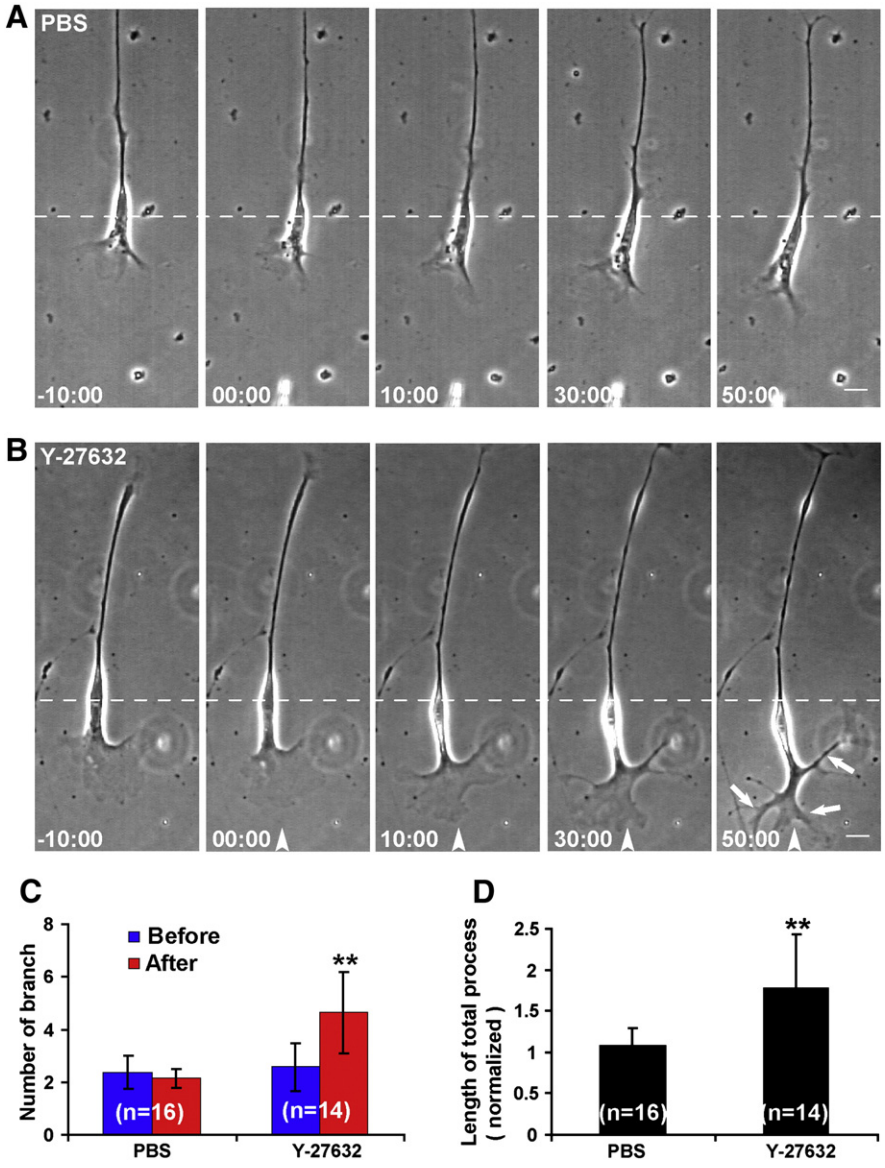

Fig. 2 – Inhibition of RhoA pathway by a gradient of Y-27632 promotes more and longer processes in OECs. (A–B) Time-lapse images show the morphological change of OECs with the process-bearing shape before and after the application of a PBS (A) or Y-27632 gradient (B). (C) A histogram shows the branch number of OECs before and after the application of a PBS or Y-27632 gradient. (D) A histogram shows the total length of processes of OECs after application of a PBS or Y-27632 gradient (normalized by before). White arrows indicate branch and white arrowheads indicate the micropipettes. Y-27632, 10 mM in micropipette. Scale bars, 20 μm. Time, minutes. We analyzed the total observed cells (PBS, n = 16; Y-27632, n = 14) from at least three independent experiments. Data are mean ± SD. $^{**}P < 0.01$, compared with control group, Student's *t* test.

mainly adopted process-bearing morphology in serum-free media and flattened morphology in serum media (Fig. 5A). Overnight exposure to Toxin-B, a general RhoGTPases inhibitor, induced the loss of flattened morphology and the development of multipolar, process-bearing morphology in a dose-dependent manner, and the process of OECs became clearly thinner and longer than control cells (Figs. 5A–B). These results suggest that RhoGTPases are involved in serum-induced morphological changes of OECs.

To further assess the role of RhoA in serum-induced morphological changes of OECs, we treated OECs under serum condition with the bacterial endotoxin C3 exoenzyme (C3), a specific RhoA inhibitor, or Y-27632, a specific ROCK inhibitor. Interestingly, we found that both C3 and Y-27632 blocked the serum-induced morphological changes of OECs in a dose-dependent manner. After treatment with C3 or Y-27632 under serum-containing media, most of OECs displayed the multi-polar and process-bearing morphology, similar to the morphology of OECs cultured under serum-free media (Figs. 5A, C–D). These results suggest that RhoA is required for serum-induced morphological changes of OECs.

Activation of RhoA by LPA promotes the morphological change of OECs from the process-bearing into flattened shape

We next examined whether the activation of RhoA is sufficient to induce the morphological changes of OECs from the process-bearing into the flattened shape. LPA has been reported to

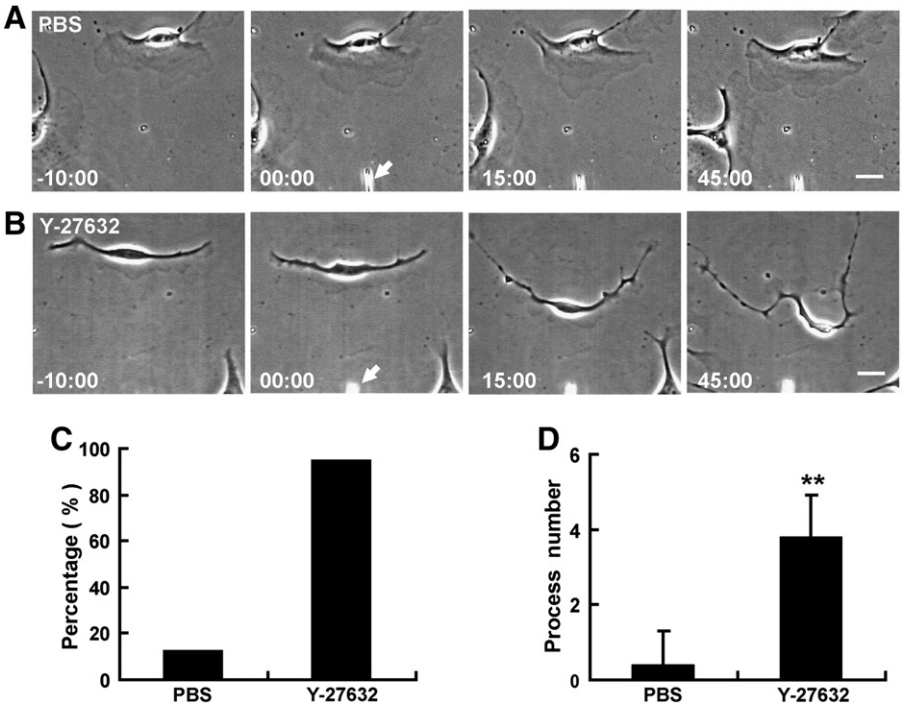

Fig. 3 – Inhibition of RhoA pathway by a gradient of Y-27632 promotes the morphological change of OECs from the flattened into process-bearing shape. (A–B) Time-lapse images show the morphological change of OECs with flattened shape before and after the application of a PBS (A) or Y-27632 gradient (B). (C) A histogram shows the percentages of changed OECs in total observed cells from three independent experiments. (D) A histogram shows the number of branch in OECs after application of a PBS (n = 24) or Y-27632 (n = 20) gradient. White arrowheads indicate the micropipettes. Scale bars, 20 μm. Time, minutes. Data are mean ± SD. **$P < 0.01$, compared with control group, Student's *t* test.

promote OEC migration by the activation of RhoA pathway [24]. Thus we tested whether LPA could induce the morphological changes of OECs from the process-bearing into the flattened shape. We first used pull-down assays to examine the activity of RhoA in cultured OECs and found that treatment with either 10% serum or 10 μM LPA resulted in marked elevation of RhoA activity in these cultured OECs (Figs. 6A–B). These results suggest that LPA or serum indeed activate RhoA. Most of OECs exhibited the multi-polar morphology with elongated processes under serum-free media. These OECs treated with LPA had shortened processes and a flattened appearance with a round shape in a dose-dependent manner. These effects of LPA on the morphology of OECs were blocked by Y-27632 (Figs. 6C–D). These results strongly suggest that the activation of RhoA by LPA is sufficient to induce the morphological changes of OECs from the process-bearing into the flattened shape.

ROCK–Myosin–F-actin as a downstream pathway of RhoA is involved in the morphological plasticity of OECs

ROCK–Myosin–F-actin is the main downstream pathway of RhoA signaling [35–37]. ROCK phosphorylates myosin light chain (MLC), which activates myosin [38–40]. Since the ROCK inhibitor Y-27632 has been shown to affect OEC morphology (Figs. 2, 3 and **5**), we next examined whether myosin and F-actin as a downstream pathway of RhoA were involved in regulation of the morphological plasticity of OECs. As shown in Figs. 7A–B, p-MLC was increased in OECs cultured in 10% serum, compared to serum-free media. These results suggest that serum indeed activates myosin. To further support this notion, Blebbistatin, a specific myosin inhibitor, was found to block serum-induced morphological changes of OECs in a dose-dependent manner (Figs. 7C, D). After treatment with Blebbistatin under serum condition, most of OECs displayed the multi-polar and process-bearing morphology, similar to the morphology of OECs cultured in serum-free media. These results suggest that myosin as a downstream of RhoA pathway is involved in serum-induced morphological plasticity of OECs.

Activation of RhoA promotes the formation of stress fibers through the ROCK–Myosin pathway and inhibition of RhoA leads to the loss of stress fibers [21,38]. To further examine whether serum induces more stress fibers in OECs through activation of RhoA, we performed F-actin staining. As shown in Fig. 7A, we found that OECs in serum-free media showed very few stress fibers. In contrast, OECs under serum-containing media showed organized bundles of actin filaments at the edge of the cells and thick parallel bundles of actin filaments that spanned the entire cell body, which obviously formed the stress fibers (Fig. 7B). These results suggested that the cytoskeletal re-organization induced by serum through activating RhoA, which may lead to the morphological change from the process-bearing into flattened shape.

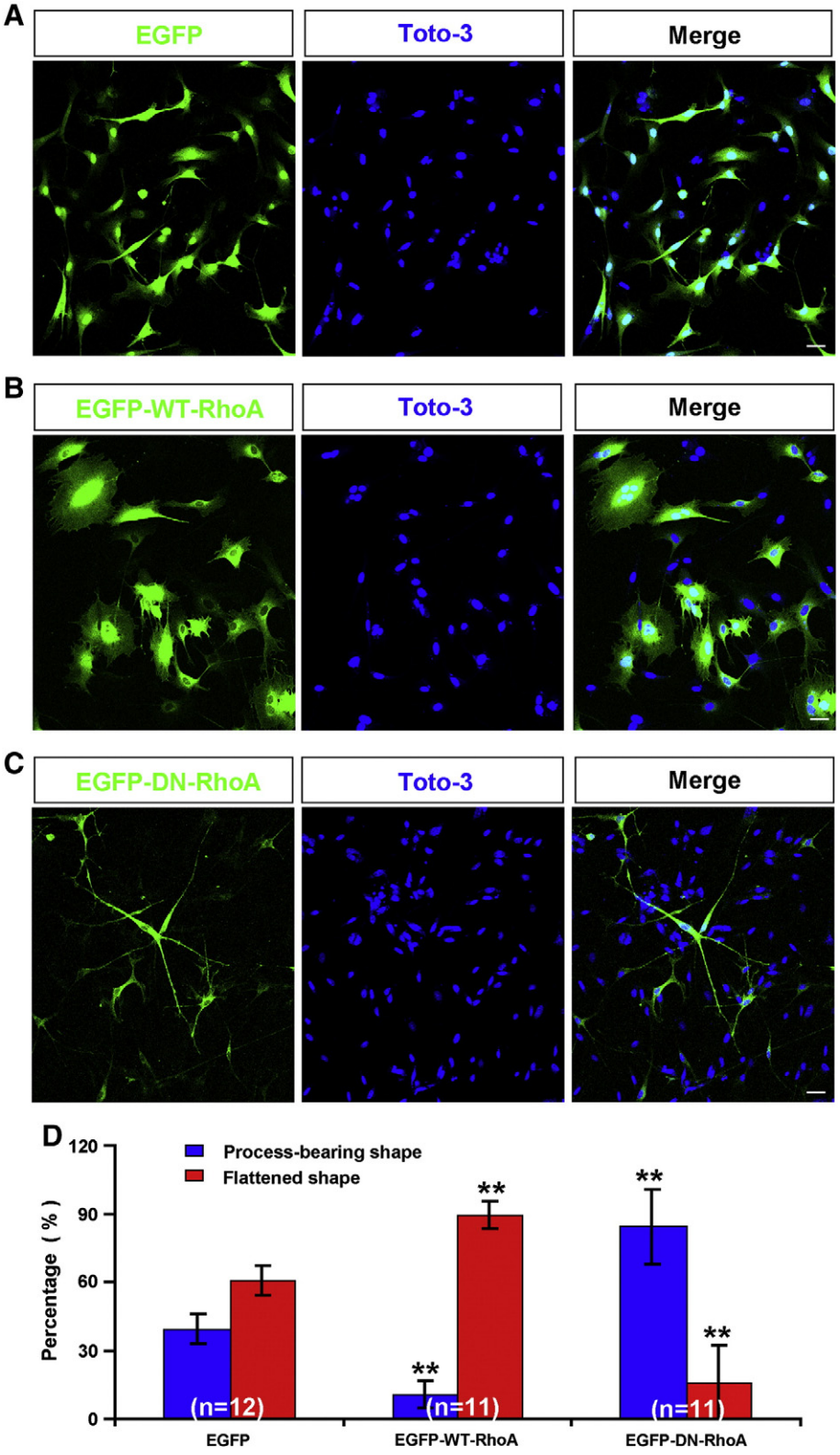

Fig. 4 – Over-expression of EGFP-WT-RhoA or EGFP-DN-RhoA affects the morphology of OECs. (A–C) Typical images show the morphology of OECs transfected with EGFP (A) or EGFP-WT-RhoA (B) or EGFP-DN-RhoA (C). Toto-3 is used to stain cellular nuclear. (D) A histogram shows the average percentages of the flattened or process-bearing OECs in total transfected cells in one field. Scale bars, 20 μm. Data are mean ± SD. $^{**}P < 0.01$, compared with control group, Student's *t* test.

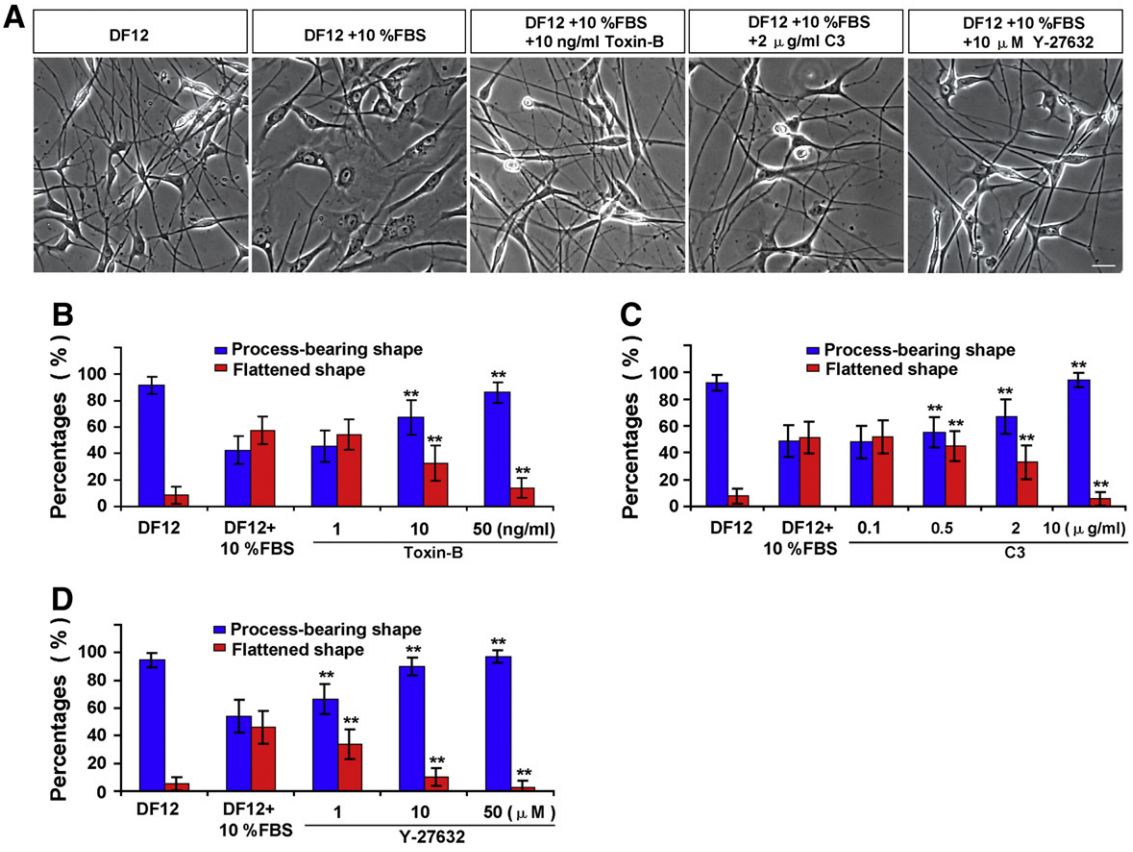

Fig. 5 – RhoA is required for serum-induced morphological change of OECs. (A) Typical images show OEC morphology under various conditions. (B–D) Histograms show the average percentages of the flattened or process-bearing OECs in total cells without or with treatment of Toxin-B (B), or C3 (C), or Y-27632 (D) under different concentrations. Scale bars, 20 μm. Data are mean ± SD. $^{**}P<0.01$ compared with DF12 + 10% FBS group, Student's *t* test.

Discussion

Cultured OECs display the morphological phenotypes with Schwann cells and astrocyte, which are described as process-bearing (Schwann cell-like) and flattened OECs (astrocyte like), respectively [4,8–12,14,15,41]. Some studies have considered the flattened phenotype as contaminating olfactory nerve fibroblasts or astrocyte [4,42]. However, recent studies have shown that OECs display morphological plasticity. Cultured OECs from olfactory bulb or mucosa have flattened and process-bearing shape. These phenotypes are immunopositive for p-75 and the reversible changes exist between these two morphological phenotypes [12,14,15]. These studies support the notion that OECs is a single cell type with morphological plasticity [13]. Consistent with these studies, in our cultured system, we found that more than 95% cultured cells displayed the double immunopositive for p-75 and S-100, or p-75 and GFAP, or S-100 and GFAP, which suggested that most of these cells were true OECs and only very few were possible contaminating fibroblasts or astrocyte. Furthermore, we found that RhoA directly regulates the morphological plasticity of cultured OECs through activating myosin and the assembly of stress fibers.

RhoGTPases act spatially and temporally to control cell shape and migration by regulating cytoskeletal re-organization. Current models postulate that Rac1 and Cdc42 promote protrusion at the leading front, whereas RhoA regulates cell contractility at cell body and contributes to the retraction of the trailing end of cells [21]. However, recent studies have shown that active RhoA displays a polarized distribution with highest activity in the front part of the cell rather than in the rear based on photometric assays of active RhoA by FRET biosensors [30,34,43,44]. Consistent with these reports, we found that the active RhoA mainly distributes in the lamellipodia and/or filopodia of OECs, but not in the soma. Interestingly, based on time-lapse imaging, we found that disruption of the active RhoA distribution by the local application of Y-27632 gradient promoted the outgrowth of process and resulted in morphological change of OECs from the flattened into process-bearing shape. These results suggest the distributions of active RhoA in the lamellipodia and/or filopodia may be critical for maintaining the morphology of OECs.

The small GTPase RhoA has been found to play an important role in the cell shape of many cell types [21]. In neurons, activation of RhoA induces the collapse of axon growth cone and cell rounding, whereas inhibition of RhoA promotes neurite outgrowth [45–47]. In astrocytes, inactivation of RhoA is a crucial step for the stellation of astrocyte [48–50]. Several studies have shown that serum free media or the protein kinase A activator dB-cAMP induce a process-bearing morphology both in astrocyte and OECs [12,14,16,18,51,52] and extracellular matrix such as laminin,

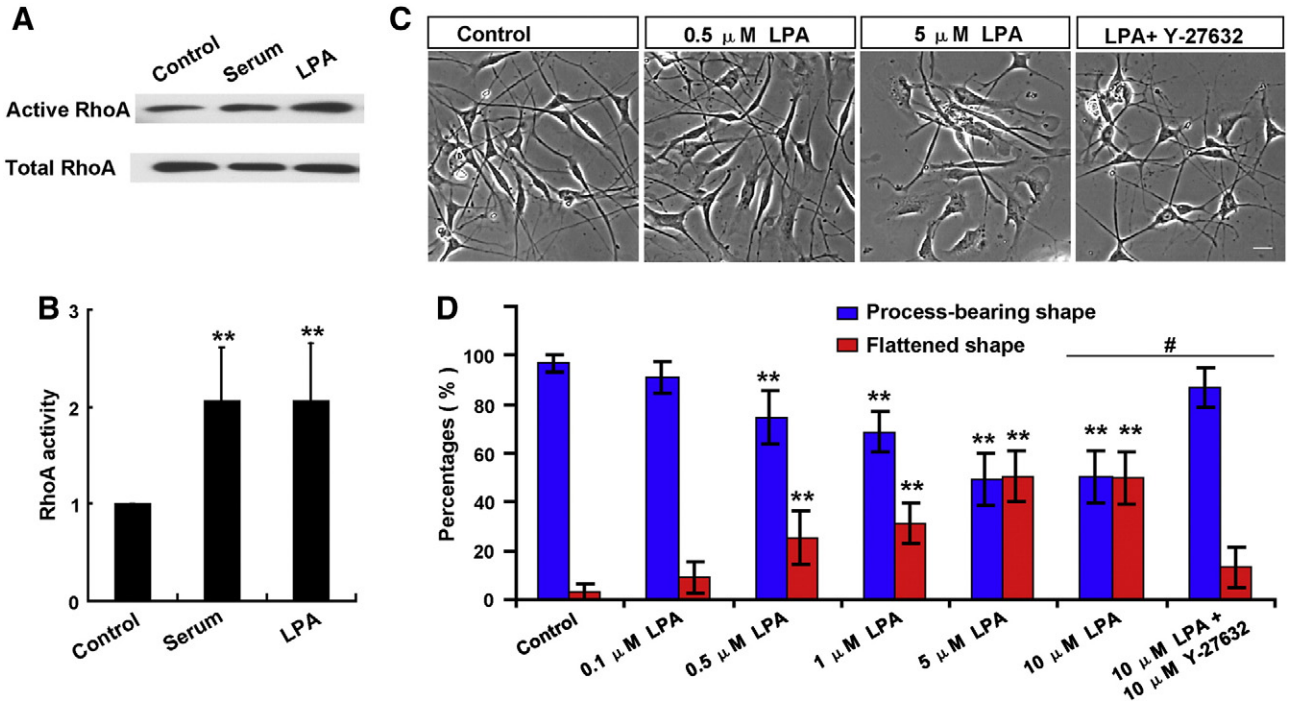

Fig. 6 – Activation of RhoA by LPA promotes the morphological change of OECs from the process-bearing into flattened shape. (A–B) Representative Western blots (A) and quantitative results (B) show the RhoA activity in response to treatment with serum (10%, 30 min) or LPA (10 μM, 30 min) in a pull-down assay. For quantitative analysis (n = 3), the ratio of active RhoA/total RhoA is normalized to the baseline level (untreated control). (C) Typical images show the OEC morphology under various conditions. (D) A histogram shows the average percentages of the flattened or process-bearing OECs in total cells under various conditions. Scale bars, 20 μm. Data are mean ± SD. $^{**}P < 0.01$ compared with control group, $^{\#}P < 0.01$ compared with 10 μM LPA group, Student's *t* test.

matrigel and fibulin-3 [19,20] also induce a process-bearing morphology of OECs. These treatments may somehow indirectly inhibit the activity of RhoA in these cells [53]. In the present study, we found that inhibitors of RhoA activity blocked serum-induced the morphological change of OECs. These results suggest that RhoA is activated by some serum components and promotes OECs to adopt the flattened shape. Furthermore, over-expression of WT-RhoA also induced OECs to adopt the flattened shape, whereas over-expression of DN-RhoA induces OECs to adopt the process-bearing shape. Whether the activation of RhoA by some physiological factor is sufficient to shorten or reduce the processes in OECs? LPA regulates the morphology of astrocyte and promote OEC migration through activating RhoA [24,48]. In our previous study, after application of the LPA gradient by single-cell migration assay, the motility of OECs was enhanced [12]. The LPA gradient can locally activate the RhoA in OECs, such as in the leading process, which makes the polarized distribution of active RhoA in processes, with the leading process exhibiting higher activity than the trailing process, and promote the migration of OECs. However, in the present study, we found that OECs in serum-free media treated with LPA in bath exhibited shortened processes, and finally became a flattened appearance with a round shape. LPA in bath can globally activate the RhoA in OECs. Thus, the local activation of RhoA promotes OEC migration in single-cell migration assay, whereas the global activation of RhoA in bath promotes the morphological changes of OECs. Taken together, we propose that RhoA activity regulates the switch of two morphological phenotypes: the activation of RhoA by some factors such as serum and LPA, induces the morphological change of OECs from the process-bearing into flattened shape, whereas the inhibition of RhoA by factors such as cAMP and C3, induces the morphological change of OECs from the flattened into process-bearing shape.

RhoA plays critical roles in cytoskeletal re-organization and is involved in the formation of stress fibers. One major downstream molecule of RhoA is ROCK, which activates myosin and induces formation of stress fibers [21,22,54,55]. Previous studies have shown that inhibition of Rho–ROCK signaling pathways promotes the outgrowth of neurite and activation of this pathway induces the retraction of neurite [45–47]. Consistent with these finding in neurons, in the present study, we found that activation of RhoA by serum induced the formation of actin stress fibers, and inhibition of RhoA–ROCK–Myosin pathways by Toxin-B, C3 or Y-27632 or Blebbistatin promoted the extension of process in OECs. These results suggest RhoA regulates the morphological plasticity of OECs through ROCK–Myosin pathways.

OECs transplantation has emerged as a very promising experimental therapy to treat axonal injuries and demyelinating diseases [3,4,6,7,56]. However, the current association of OEC morphology with functional phenotype is questionable. Several studies have shown that the process-bearing (Schwann cell-like) shape of OECs myelinate central axons in lesion environments, and myelinate, ensheath and support outgrowth of neurite in culture [4,57–61],

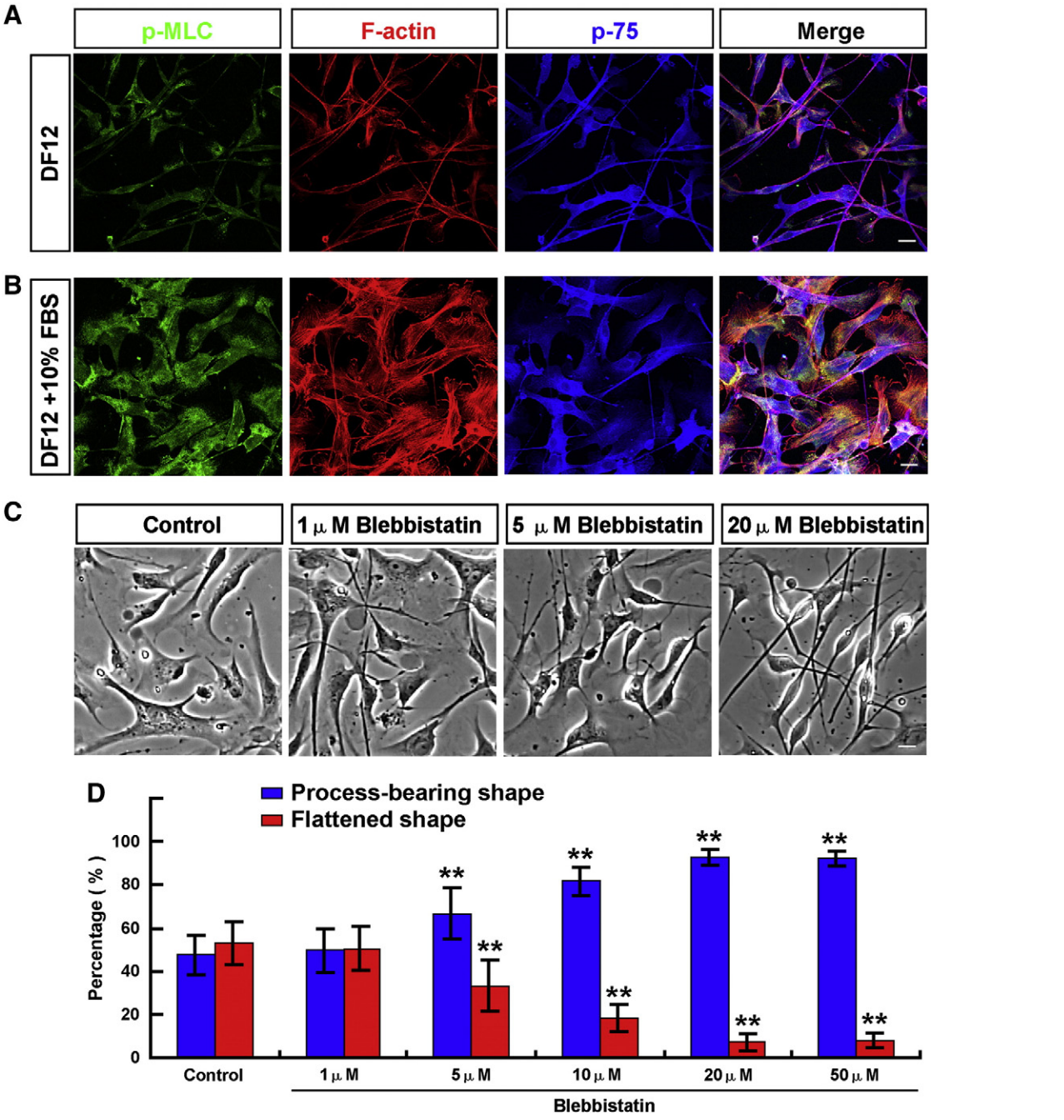

Fig. 7 – ROCK-Myosin-F-actin as a downstream pathway of RhoA is involved in morphological plasticity of OECs. (A–B) Triple immuno-staining of OECs for p-MLC (green), F-actin (red) and p-75 (blue) under cultured condition with (B) or without serum media (A). (C) Typical images show OEC morphology under various conditions. (D) A histogram shows the average percentages of the flattened or the process-bearing OECs in total cells under various conditions. Scale bars, 20 μm. Data are mean ± SD. $^{**}P<0.01$ compared with control group, Student's *t* test.

and the flattened shape of OECs (astrocyte-like OECs or fibroblast-like OECs) are supportive cells or contaminating cells or immature cells [4,10,62]. However, other studies have showed that the reversible change exist between these two morphological phenotypes in culture [12,14,15]. OECs can adopt different morphology according to changing conditions or new environments. In the present study, we found that RhoA pathway regulates the morphological plasticity of OECs. Further studies should be carried to ascertain whether a particular morphology of OECs is associated with a regeneration-promoting phenotype.

Supplementary materials related to this article can be found online at doi:10.1016/j.yexcr.2011.09.004.

Acknowledgments

This study was supported by the Startup Foundation (QTJ09013), Wenzhou Science & Technology Bureau (H20100065), 5010 Program (XNK07006) of Wenzhou Medical School, Natural Science Foundation of Zhejiang Province (Y2110242, Y2110364), the National Natural Science Foundation (30770657, 81100903), National Key Basic Research Program (2007CB947100, 2011CB504401), and the Ministry of Science and Technology of China (2009ZX09311-001).

REFERENCES

[1] G. Raisman, Y. Li, Repair of neural pathways by olfactory ensheathing cells, Nat. Rev. Neurosci. 8 (2007) 312–319.
[2] E.H. Franssen, F.M. de Bree, J. Verhaagen, Olfactory ensheathing glia: their contribution to primary olfactory nervous system regeneration and their regenerative potential following transplantation into the injured spinal cord, Brain Res. Rev. 56 (2007) 236–258.
[3] T. Kato, O. Honmou, T. Uede, K. Hashi, J.D. Kocsis, Transplantation of human olfactory ensheathing cells elicits remyelination of demyelinated rat spinal cord, Glia 30 (2000) 209–218.
[4] Y. Li, P.M. Field, G. Raisman, Regeneration of adult rat corticospinal axons induced by transplanted olfactory ensheathing cells, J. Neurosci. 18 (1998) 10514–10524.
[5] Z. Su, C. He, Olfactory ensheathing cells: biology in neural development and regeneration, Prog. Neurobiol. 92 (2010) 517–532.
[6] A. Ramon-Cueto, C. Munoz-Quiles, Clinical application of adult olfactory bulb ensheathing glia for nervous system repair, Exp. Neurol. 229 (2011) 181–194.
[7] A. Mackay-Sim, J.A. St John, Olfactory ensheathing cells from the nose: clinical application in human spinal cord injuries, Exp. Neurol. 229 (2011) 174–180.
[8] A. Ramon-Cueto, M. Nieto-Sampedro, Glial cells from adult rat olfactory bulb: immunocytochemical properties of pure cultures of ensheathing cells, Neuroscience 47 (1992) 213–220.
[9] E. Au, A.J. Roskams, Olfactory ensheathing cells of the lamina propria in vivo and in vitro, Glia 41 (2003) 224–236.
[10] I.A. Franceschini, S.C. Barnett, Low-affinity NGF-receptor and E-N-CAM expression define two types of olfactory nerve ensheathing cells that share a common lineage, Dev. Biol. 173 (1996) 327–343.
[11] S.K. Pixley, The olfactory nerve contains two populations of glia, identified both in vivo and in vitro, Glia 5 (1992) 269–284.
[12] Z.H. Huang, Y. Wang, L. Cao, Z.D. Su, Y.L. Zhu, Y.Z. Chen, X.B. Yuan, C. He, Migratory properties of cultured olfactory ensheathing cells by single-cell migration assay, Cell Res. 18 (2008) 479–490.
[13] A.J. Vincent, A.K. West, M.I. Chuah, Morphological and functional plasticity of olfactory ensheathing cells, J. Neurocytol. 34 (2005) 65–80.
[14] A.J. Vincent, A.K. West, M.I. Chuah, Morphological plasticity of olfactory ensheathing cells is regulated by cAMP and endothelin-1, Glia 41 (2003) 393–403.
[15] A.N. van den Pol, J.G. Santarelli, Olfactory ensheathing cells: time lapse imaging of cellular interactions, axonal support, rapid morphologic shifts, and mitosis, J. Comp. Neurol. 458 (2003) 175–194.
[16] R. Doucette, R. Devon, Elevated intracellular levels of cAMP induce olfactory ensheathing cells to express GAL-C and GFAP but not MBP, Glia 13 (1995) 130–140.
[17] C.L. Alexander, U.F. Fitzgerald, S.C. Barnett, Identification of growth factors that promote long-term proliferation of olfactory ensheathing cells and modulate their antigenic phenotype, Glia 37 (2002) 349–364.
[18] Y. Wang, Z.H. Huang, cAMP mediates the morphological change of cultured olfactory ensheathing cells induced by serum, Sheng Li Xue Bao 63 (2011) 31–38.
[19] K.T. Tisay, B. Key, The extracellular matrix modulates olfactory neurite outgrowth on ensheathing cells, J. Neurosci. 19 (1999) 9890–9899.
[20] J. Vukovic, M.J. Ruitenberg, K. Roet, E. Franssen, A. Arulpragasam, T. Sasaki, J. Verhaagen, A.R. Harvey, S.J. Busfield, G.W. Plant, The glycoprotein fibulin-3 regulates morphology and motility of olfactory ensheathing cells in vitro, Glia 57 (2009) 424–443.
[21] S. Etienne-Manneville, A. Hall, Rho GTPases in cell biology, Nature 420 (2002) 629–635.
[22] K.A. DeMali, K. Burridge, Coupling membrane protrusion and cell adhesion, J. Cell Sci. 116 (2003) 2389–2397.
[23] Z. Su, L. Cao, Y. Zhu, X. Liu, Z. Huang, A. Huang, C. He, Nogo enhances the adhesion of olfactory ensheathing cells and inhibits their migration, J. Cell Sci. 120 (2007) 1877–1887.
[24] H. Yan, D. Lu, S.A. Rivkees, Lysophosphatidic acid regulates the proliferation and migration of olfactory ensheathing cells in vitro, Glia 44 (2003) 26–36.
[25] Z.H. Huang, Y. Wang, Z.D. Su, J.G. Geng, Y.Z. Chen, X.B. Yuan, C. He, Slit-2 repels the migration of olfactory ensheathing cells by triggering Ca^{2+}-dependent cofilin activation and RhoA inhibition, J. Cell Sci. 124 (2011) 186–197.
[26] S.C. Barnett, A.J. Roskams, Olfactory ensheathing cells. Isolation and culture from the rat olfactory bulb, Methods Mol. Biol. 198 (2002) 41–48.
[27] L. Cao, Z. Su, Q. Zhou, B. Lv, X. Liu, L. Jiao, Z. Li, Y. Zhu, Z. Huang, A. Huang, C. He, Glial cell line-derived neurotrophic factor promotes olfactory ensheathing cells migration, Glia 54 (2006) 536–544.
[28] Y. Zhu, L. Cao, Z. Su, L. Mu, Y. Yuan, L. Gao, Y. Qiu, C. He, Olfactory ensheathing cells: attractant of neural progenitor migration to olfactory bulb, Glia 58 (2010) 716–729.
[29] L. Cao, Y.L. Zhu, Z. Su, B. Lv, Z. Huang, L. Mu, C. He, Olfactory ensheathing cells promote migration of Schwann cells by secreted nerve growth factor, Glia 55 (2007) 897–904.
[30] H. Yoshizaki, Y. Ohba, K. Kurokawa, R.E. Itoh, T. Nakamura, N. Mochizuki, K. Nagashima, M. Matsuda, Activity of Rho-family GTPases during cell division as visualized with FRET-based probes, J. Cell Biol. 162 (2003) 223–232.
[31] J.N. Feige, D. Sage, W. Wahli, B. Desvergne, L. Gelman, PixFRET, an ImageJ plug-in for FRET calculation that can accommodate variations in spectral bleed-throughs, Microsc. Res. Tech. 68 (2005) 51–58.
[32] G. Fu, H.Y. Yang, C. Wang, F. Zhang, Z.D. You, G.Y. Wang, C. He, Y.Z. Chen, Z.Z. Xu, Detection of constitutive heterodimerization of the integrin Mac-1 subunits by fluorescence resonance energy transfer in living cells, Biochem. Biophys. Res. Commun. 346 (2006) 986–991.
[33] F. Zhang, G. Fu, C. Wang, L. Cao, H.Y. Yang, G.Y. Wang, Y.Z. Chen, C. He, Detection of homo- or hetero-association of Doks by fluorescence resonance energy transfer in living cells, Mol. Imaging Biol. 11 (2009) 188–194.
[34] C.B. Guan, H.T. Xu, M. Jin, X.B. Yuan, M.M. Poo, Long-range Ca(2+) signaling from growth cone to soma mediates reversal of neuronal migration induced by slit-2, Cell 129 (2007) 385–395.
[35] K. Bhadriraju, M. Yang, S. Alom Ruiz, D. Pirone, J. Tan, C.S. Chen, Activation of ROCK by RhoA is regulated by cell adhesion, shape, and cytoskeletal tension, Exp. Cell Res. 313 (2007) 3616–3623.
[36] R. Samaniego, L. Sanchez-Martin, A. Estecha, P. Sanchez-Mateos, Rho/ROCK and myosin II control the polarized distribution of endocytic clathrin structures at the uropod of moving T lymphocytes, J. Cell Sci. 120 (2007) 3534–3543.
[37] A.J. Ridley, M.A. Schwartz, K. Burridge, R.A. Firtel, M.H. Ginsberg, G. Borisy, J.T. Parsons, A.R. Horwitz, Cell migration: integrating signals from front to back, Science 302 (2003) 1704–1709.
[38] G. Totsukawa, Y. Yamakita, S. Yamashiro, D.J. Hartshorne, Y. Sasaki, F. Matsumura, Distinct roles of ROCK (Rho-kinase) and MLCK in spatial regulation of MLC phosphorylation for assembly

of stress fibers and focal adhesions in 3T3 fibroblasts, J. Cell Biol. 150 (2000) 797–806.
[39] A. Yoneda, H.A. Multhaupt, J.R. Couchman, The Rho kinases I and II regulate different aspects of myosin II activity, J. Cell Biol. 170 (2005) 443–453.
[40] R. Minambres, R.M. Guasch, A. Perez-Arago, C. Guerri, The RhoA/ROCK-I/MLC pathway is involved in the ethanol-induced apoptosis by anoikis in astrocytes, J. Cell Sci. 119 (2006) 271–282.
[41] R.J. Franklin, J.M. Gilson, I.A. Franceschini, S.C. Barnett, Schwann cell-like myelination following transplantation of an olfactory bulb-ensheathing cell line into areas of demyelination in the adult CNS, Glia 17 (1996) 217–224.
[42] Y. Li, P. Decherchi, G. Raisman, Transplantation of olfactory ensheathing cells into spinal cord lesions restores breathing and climbing, J. Neurosci. 23 (2003) 727–731.
[43] K. Kurokawa, M. Matsuda, Localized RhoA activation as a requirement for the induction of membrane ruffling, Mol. Biol. Cell 16 (2005) 4294–4303.
[44] O. Pertz, L. Hodgson, R.L. Klemke, K.M. Hahn, Spatiotemporal dynamics of RhoA activity in migrating cells, Nature 440 (2006) 1069–1072.
[45] M. Hirose, T. Ishizaki, N. Watanabe, M. Uehata, O. Kranenburg, W.H. Moolenaar, F. Matsumura, M. Maekawa, H. Bito, S. Narumiya, Molecular dissection of the Rho-associated protein kinase (p160ROCK)-regulated neurite remodeling in neuroblastoma N1E-115 cells, J. Cell Biol. 141 (1998) 1625–1636.
[46] K. Jalink, E.J. van Corven, T. Hengeveld, N. Morii, S. Narumiya, W.H. Moolenaar, Inhibition of lysophosphatidate- and thrombin-induced neurite retraction and neuronal cell rounding by ADP ribosylation of the small GTP-binding protein Rho, J. Cell Biol. 126 (1994) 801–810.
[47] O. Kranenburg, M. Poland, F.P. van Horck, D. Drechsel, A. Hall, W.H. Moolenaar, Activation of RhoA by lysophosphatidic acid and Galpha12/13 subunits in neuronal cells: induction of neurite retraction, Mol. Biol. Cell 10 (1999) 1851–1857.
[48] G.J. Ramakers, W.H. Moolenaar, Regulation of astrocyte morphology by RhoA and lysophosphatidic acid, Exp. Cell Res. 245 (1998) 252–262.
[49] C.J. Chen, Y.C. Ou, S.Y. Lin, S.L. Liao, Y.S. Huang, A.N. Chiang, L-glutamate activates RhoA GTPase leading to suppression of astrocyte stellation, Eur. J. Neurosci. 23 (2006) 1977–1987.
[50] M. Burgos, S. Calvo, F. Molina, C.F. Vaquero, A. Samarel, J. Llopis, P. Tranque, PKCepsilon induces astrocyte stellation by modulating multiple cytoskeletal proteins and interacting with Rho A signalling pathways: implications for neuroinflammation, Eur. J. Neurosci. 25 (2007) 1069–1078.
[51] J.E. Goldman, B. Abramson, Cyclic AMP-induced shape changes of astrocytes are accompanied by rapid depolymerization of actin, Brain Res. 528 (1990) 189–196.
[52] S. Safavi-Abbasi, J.R. Wolff, M. Missler, Rapid morphological changes in astrocytes are accompanied by redistribution but not by quantitative changes of cytoskeletal proteins, Glia 36 (2001) 102–115.
[53] S.M. Lim, B.A. Kreipe, J. Trzeciakowski, L. Dangott, A. Trache, Extracellular matrix effect on RhoA signaling modulation in vascular smooth muscle cells, Exp. Cell Res. 316 (2010) 2833–2848.
[54] A. Hall, Rho GTPases and the actin cytoskeleton, Science 279 (1998) 509–514.
[55] A.J. Ridley, Rho GTPases and cell migration, J. Cell Sci. 114 (2001) 2713–2722.
[56] C. Munoz-Quiles, F.F. Santos-Benito, M.B. Llamusi, A. Ramon-Cueto, Chronic spinal injury repair by olfactory bulb ensheathing glia and feasibility for autologous therapy, J. Neuropathol. Exp. Neurol. 68 (2009) 1294–1308.
[57] R. Kumar, S. Hayat, P. Felts, S. Bunting, C. Wigley, Functional differences and interactions between phenotypic subpopulations of olfactory ensheathing cells in promoting CNS axonal regeneration, Glia 50 (2005) 12–20.
[58] R. Devon, R. Doucette, Olfactory ensheathing cells myelinate dorsal root ganglion neurites, Brain Res. 589 (1992) 175–179.
[59] A. Ramon-Cueto, J. Perez, M. Nieto-Sampedro, In vitro enfolding of olfactory neurites by p75 NGF receptor positive ensheathing cells from adult rat olfactory bulb, Eur. J. Neurosci. 5 (1993) 1172–1180.
[60] J.D. Kocsis, K.L. Lankford, M. Sasaki, C. Radtke, Unique in vivo properties of olfactory ensheathing cells that may contribute to neural repair and protection following spinal cord injury, Neurosci. Lett. 456 (2009) 137–142.
[61] A. Perez-Bouza, C.B. Wigley, W. Nacimiento, J. Noth, G.A. Brook, Spontaneous orientation of transplanted olfactory glia influences axonal regeneration, Neuroreport 9 (1998) 2971–2975.
[62] R.J. Sonigra, P.C. Brighton, J. Jacoby, S. Hall, C.B. Wigley, Adult rat olfactory nerve ensheathing cells are effective promoters of adult central nervous system neurite outgrowth in coculture, Glia 25 (1999) 256–269.